Cu2ZnSnS x O4 x and Cu2ZnSnS x Se4 x : First principles simulations of optimal alloy configurations and their energies

Chaochao Dun, N. A. W. Holzwarth, Yuan Li, Wenxiao Huang, and David L. Carroll

Citation: Journal of Applied Physics **115**, 193513 (2014); doi: 10.1063/1.4876447
View online: http://dx.doi.org/10.1063/1.4876447
View Table of Contents: http://scitation.aip.org/content/aip/journal/jap/115/19?ver=pdfcov
Published by the AIP Publishing

$Cu_2ZnSnS_xO_{4-x}$ and $Cu_2ZnSnS_xSe_{4-x}$: First principles simulations of optimal alloy configurations and their energies

Chaochao Dun,[1] N. A. W. Holzwarth,[2,a)] Yuan Li,[1] Wenxiao Huang,[1] and David L. Carroll[1]
[1]*Center for Nanotechnology and Molecular Materials, Department of Physics, Wake Forest University, Winston-Salem, North Carolina 27109, USA*
[2]*Department of Physics, Wake Forest University, Winston-Salem, North Carolina 27109, USA*

(Received 24 March 2014; accepted 1 May 2014; published online 21 May 2014)

With the aim of exploring oxidation and selenization of the photovoltaic material Cu_2ZnSnS_4, we used first principles methods to study the structure and stability of $Cu_2ZnSnS_xO_{4-x}$ and $Cu_2ZnSnS_xSe_{4-x}$ alloys for $0 \le x \le 4$. Pure Cu_2ZnSnO_4 was found to have the lowest heat of formation, followed by Cu_2ZnSnS_4, and finally $Cu_2ZnSnSe_4$. This suggests that oxidization is very likely to occur, whereas selenization can only be accomplished under high temperature. For the alloys, the energetically favorable chalcogen configurations are very different for oxygen and selenium. While the energies of the selenium alloys are insensitive to the distribution of S and Se configurations, the lowest energy oxygen alloys have alternating S and O sites in the *a–b* planes. In considering the heats of formation of the $Cu_2ZnSnS_xO_{4-x}$ alloys, we find that they are unstable with respect to decomposition into binary oxides and sulfides except for small concentrations of O. Our results also show that it is energetically more favorable to sulfurize $Cu_2ZnSnSe_4$ than to selenize Cu_2ZnSnS_4. © *2014 AIP Publishing LLC*. [http://dx.doi.org/10.1063/1.4876447]

I. INTRODUCTION

Key to the success of solar energy production is the development of thin film photovoltaic devices with high efficiency and low cost. As an absorber layer in thin film solar cells, multicomponent copper chalcogenide based compounds, namely, Cu_2ZnSnS_4(CZTS) and $Cu_2ZnSnSe_4$ (CZTSe) have drawn much attention because of their abundant and non-toxic elements, as well as their direct band gap, which matches well with the solar spectrum.[1–4] So far, the best pure sulphide CZTS device has reported an efficiency of 8.4%,[5] whereas the best pure selenide CZTSe device has reported a higher efficiency of 9.7%.[6] However, such performance is far below the theoretical limit (32.4% and 31.0% for CZTS and CZTSe, respectively) for the single-junction devices.[7] Recently, a considerable enhancement in power conversion efficiency was achieved by the selenization of CZTS films, increasing the efficiency to 12.6%.[8] This encouraging outcome has inspired a new approach to producing higher efficiency solar cells in the study of the alloy system $Cu_2ZnSnS_xSe_{4-x}$ (CZTSSe).[9–11]

Because of their technological promise, CZTS, CZTSe, and CZTSSe have received substantial experimental and computational attention. One important related research area which has received less attention is that of the role of oxygen in these materials. Under most circumstances, the CZTS family of materials and devices is protected from oxygen during synthesis and in device operational conditions. However, there have been a few recent experimental and computational reports[12–14] on the synthesis and use of Cu_2ZnSnO_4 (CZTO) and its alloys $Cu_2ZnSnS_xO_{4-x}$ (CZTSO). For example, Washio *et al*. reported the fabrication of CZTS-based thin film solar cells using CZTSO precursors, resulting in devices with 6% efficiency.[13] The range of effects of oxygen on CZTS technology (both the beneficial and the detrimental) remains an open question.

Computer simulations have played an important part in the development of the CZTS family of materials and related devices.[15–29] Both O and Se are chalcogens, which can substitute for S without changing the valence of the other elements. In the present work, we extend the computational effort to study the effects of oxygen on CZTS, including the study of optimal structures of pure CZTO and of the CZTSO alloys and their energies, using a parallel study of pure CZTS and of the CZTSSe alloys as a guiding reference.

The organization of the paper is as follows. Section II briefly outlines the computational methods used in the present work. Section III presents the detailed results including the structural properties of the pure materials (Sec. III A), their heats of formation (Sec. III B), and the structural and energetic properties of the CZTSO and CZTSSe alloys (Sec. III C). The summary and conclusions are presented in Sec. IV. Some details of the results are presented in the Appendix.

II. CALCULATIONAL METHODS

The calculations reported in this paper are based on density functional theory (DFT),[30,31] using the local density approximation (LDA)[32] for the exchange-correlation functional. The calculations were carried out using the projector augmented wave (PAW)[33] formalism as implemented in the *Quantum Espresso*[34] and *abinit*[35] packages. The PAW basis and projector functions were generated by the *atompaw* code.[36] The plane wave expansion of the wavefunctions (in terms of the wave vector **k** and reciprocal lattice vector **G**) was found to be well-converged within the cut-off criterion

a)Electronic mail: natalie@wfu.edu

of $|\mathbf{k}+\mathbf{G}| \leq 8\,\text{bohr}^{-1}$. The **k**-point sampling volume was less than 0.01 bohr^{-3}. Internal tests estimate the numerical errors for energy to be within 0.002 eV/unit cell and the numerical error for lattice constants to be within 0.03 Å. The analysis of the results benefited from several visualization packages including XCRYSDEN (Ref. 37) and VESTA.[38] For the simulations of the S-O and S-Se alloy materials, supercell techniques were used as discussed in Sec. III C.

III. RESULTS AND DISCUSSION

A. Structural properties of pure CZTS, CZTSe, and CZTO

The structural properties of Cu_2ZnSnS_4 and $Cu_2ZnSnSe_4$ have been well studied with both experiments and simulations. The two most common crystalline forms[44] are kesterite (KS) ($I\bar{4}$, space group No. 82) and stannite (ST) ($I\bar{4}2m$, space group No. 121).[45] There has been some controversy over details of the structures since the two forms are very similar (the $I\bar{4}$ space group is a subgroup of $I\bar{4}2m$), differing primarily in arrangement of Zn and Cu sites. Depending on sample preparation methods, there can be disorder on the Cu and Zn sites as observed by recent nuclear magnetic resonance (NMR) analysis.[46] In fact, it has been recognized that X-ray diffraction analysis[2,47] alone is not accurate enough to distinguish between the KS and ST structures because Zn and Cu have very similar X-ray form factors. While for device development, a wide variety of synthesis techniques and morphologies have been studied including nano-scaled powders and thin films, for purposes of comparing with first principles simulations of the ideal structures, single crystal samples are of the greatest interest. Nearly, defect-free single crystals of KS-Cu_2ZnSnS_4 materials have been grown.[39,42] Single crystal samples of KS-$Cu_2ZnSnSe_4$ have been reported,[48] although single crystal samples of ST-$Cu_2ZnSnSe_4$ have also been reported.[41] While there are a few experimental and computational reports[12–14] on Cu_2ZnSnO_4, a detailed analysis of the stability and structures of Cu_2ZnSnO_4 has not previously been reported.

There have also been a large number of numerical simulations concerning the CZTS family.[15–29] In general, the results obtained using the LDA exchange-correlation functional[32] tend to uniformly underestimate the experimental lattice constants by 2%, while those obtained using the GGA exchange-correlation functional[49,50] normally overestimate the experimental lattice constants by 1%. Calculations using the hybrid HSE functional[51] obtain structural parameters very close to those of the GGA results.[15,16,23]

In the present study, calculations were performed using the LDA exchange-correlation functional and assuming the ideal kesterite and stannite forms of CZTS, CZTSe, and CZTO. The results of the calculated lattice parameters and non-equivalent fractional coordinates of the S/Se/O sites are listed in Table I together with representative experimental measurements and previous LDA calculations. Generally, the present results are in excellent agreement with previous calculations within the expected accuracy of the calculations. While the calculated lattice constants are 2% smaller than the experimental values, the relative lattice sizes and the internal structural parameters agree with the experimental results within 1%, providing confidence that the method is reliable for modeling the structural and energetic properties of these materials in their electronic ground states. Of course, additional effort is needed to model the optical properties and to estimate band gaps.[15,23,52]

TABLE I. Crystalline parameters for pure CZTS/Se/O in their kesterite and stannite structures. Results of the lattice constants *a* and *c* as well as the fractional coordinates for S/Se/O sites are listed, comparing results of the present work with previous work and experimental measurements.

	Cu_2ZnSnS_4		$Cu_2ZnSnSe_4$		Cu_2ZnSnO_4	
	Kesterite	Stannite	Kesterite	Stannite	Kesterite	Stannite
a (Å)	5.330[a]	5.326[a]	5.607[a]	5.606[a]	4.622[a]	4.599[a]
	5.421[b]	5.325[c]	5.610[d]	5.688[e], 5.684[f]		
	5.417[g,h]		5.624[i]	5.622[i]		
c (Å)	10.656[a]	10.667[a]	11.205[a]	11.205[a]	9.155[a]	9.232[a]
	10.812[b]	10.629[c]	11.280[d]	11.338[e], 11.353[f]		
	10.790[g,h]		11.264[i]	11.267[i]		
Fractional (*x*, *y*, *z*) coordinates of S/Se/O sites						
X	0.759[a]	0.759[a]	0.760[a]	0.760[a]	0.762[a]	0.753[a]
	0.756[j]	0.760[c]	0.761[c]	0.759[e]		
	0.755[g]		0.757[k]	0.757[k]		
Y	0.763[a]	0.759[a]	0.769[a]	0.760[a]	0.754[a]	0.753[a]
	0.757[j]	0.760[c]	0.771[c]	0.759[e]		
	0.755[g]		0.767[k]	0.757[k]		
Z	0.870[a]	0.866[a]	0.869[a]	0.865[a]	0.873[a]	0.880[a]
	0.872[j]	0.865[c]	0.869[c]	0.871[e]		
	0.872[g]		0.871[k]	0.865[k]		

[a]Present work.
[b]Experiment (nano crystals) from Ref. 2.
[c]Calculation from Ref. 19.
[d]Experiment (nano crystals) from Ref. 10.
[e]Experiment (single crystals) from Ref. 41.
[f]Experiment (poly crystalline) from Ref. 43.
[g]Experiment (single crystals) from Ref. 39.
[h]Experiment (single crystals) from Ref. 42.
[i]Calculation from Ref. 25.
[j]Experiment (single crystals) from Ref. 40.
[k]Calculation from Ref. 20.

The similarity of the lattice parameters and the positions of the S sites in the kesterite and stannite structures of CZTS have been well-reported in the literature;[44] as shown in Table I, the kesterite/stannite similarity is also found in CZTSe and CZTO.

B. Heat of formation of CZTS, CZTSe, CZTO, and related materials

An important result from computer optimization of various crystals is the assessment of relative stabilities for the idealized structures, which is most easily quantified in terms of the heats of formation ΔH. The heat of formation for each compound material is defined as its enthalpy relative to the energy of its elemental constituents in their standard forms as defined in the CRC Handbook[53] or the NIST JANAF Thermodynamic Tables.[54] A reasonable approximation to ΔH can be determined from the zero temperature total self-consistent energy results from the Kohn-Sham calculations.

In this study, the reference states for the elements are solid Cu in the face-centered cubic (*fcc*) structure, solid Zn in the hexagonal closest-packed (*hcp*) structure, solid (white) Sn in diamond structure, solid S in the α-S structure (*Fddd* with space group No. 70), and solid Se in the trigonal form with the space group $P3_121$ (No. 152). These elemental reference states were simulated directly. The standard enthalpy for O is its gaseous molecular form. Since the computational methods perform less well on molecular systems, we used a semi-empirical approach following the method of Wang *et al.*[56] In this case, the reference energy for O was determined by performing a least-squares fit to the enthalpy results of several oxygen-containing compounds of Cu, Zn, S, Zn, and Se listed in the CRC Handbook[53] and the NIST JANAF Thermodynamic Tables.[54] This approach has been successfully used to study the energetics of other families of materials.[57]

The heats of formation for the CZTS family of materials are presented in Tables II and III, comparing the results of the present work with results reported in the literature. These results for the heats of formation serve several purposes. The first question is to determine relative stabilities of the CZTS, CZTSe, and CZTO materials in the kesterite and stannite structures. Second, the comparison of the present results with experiment and with previous computations can provide a useful assessment of the validity of the computational methods and physical approximations. Third, the heat of formation results can be used to estimate the thermodynamic stability and meta-stability of the various compositions and crystalline phases relative to various decomposition products.

1. Relative stabilities of the kesterite and stannite crystal structures

As shown in Tables II and III, the kesterite structure has the lower energy for all three materials CZTS, CZTSe, and CZTO compared to the stannite structure. However, the energy difference between the two structures is very small—approximately 3 meV per atom—for each of the S-based, Se-based, and O-based compounds. Previous simulations reported in the literature provided similar results[15–17,19,24] (within a few meV/atom) for CZTS and CZTSe. Here, we see that CZTO follows this trend as well. The very small energy difference between the kesterite and stannite structures indicates that the Cu/Zn disorder may occur under certain growth conditions, which has been observed experimentally from neutron diffraction[58] and NMR (Ref. 46) measurements.

TABLE II. Summary of heats of formation results for CZTSO and related materials in units of eV per formula unit. For each formula unit given in the first column, the space-group symbol and number is listed in the second column. The heat formation ΔH_{cal} calculated in the present optimization study is given in the third column. When available, literature values of heats of formation from calculation (ΔH_{cal}) and experiment (ΔH_{exp}) are listed in columns of four and five, respectively. In general, the detailed crystal structures corresponding to the experimental ΔH_{exp} are not known. Compounds indicated with * were used in fitting the O_2 reference energies as explained in the text.

Formula unit	Crystal structure	ΔH_{cal} (Present work)	ΔH_{cal} (Literature)	ΔH_{exp} (Literature)
CuO*	*C*2/*c* (No. 15)	−1.645	…	−1.630,[a] −1.617,[b] −1.677[c]
Cu_2O*	$Pn\bar{3}m$ (No. 224)	−1.756	…	−1.747,[a] −1.769,[b] −1.795[c]
ZnO*	$P6_3mc$ (No. 186)	−3.410	…	−3.633[a]
SnO*	*P*4/*nmn* (No. 129)	−2.949	…	−2.909[a]
SnO_2*	$P6_3mc$ (No. 186)	−5.788	…	−5.987[a]
CuS	$P6_3/mmc$ (No. 194)	−0.705	−0.49[d]	…
CuS	*Cmcm* (No. 63)	−0.712	…	−0.550,[a] −0.542[c]
CuS_2	$Pa\bar{3}$ (No. 205)	−0.874	…	…
Cu_2S	$P4_32_12$ (No. 96)	−0.923	…	…
Cu_2S	$P2_1/c$ (No. 14)	−0.931	−0.52[d]	−0.823,[a] −0.824[c]
ZnS	$F\bar{4}3m$ (No. 216)	−1.774	−1.75[d]	−1.996,[a] −2.127[c]
SnS	*Pnma* (No. 62)	−1.072	−1.01,[d] −1.03[e]	−1.036,[a] −1.118[c]
SnS_2	$P\bar{3}m1$ (No. 164)	−1.320	−1.33,[d] −1.36[e]	−1.592[c]
Sn_2S_3	*Pnma* (No. 62)	−2.353	−2.39[e]	−2.732[c]
SO_3*	$Pna2_1$ (No. 33)	−5.089	…	−4.711[a]
$CuSO_4$*	*Pnma* (No. 62)	−7.849	…	−7.995,[a] −7.980[b]
$ZnSO_4$*	*Pnma* (No. 62)	−10.207	…	−10.186,[a] −10.158,[b] −10.171[c]
Cu_2SnO_3	*Cc* (No. 9)	−5.938	…	…
Cu_2SnS_3	*Cc* (No. 9)	−2.680	−2.36[d]	…
KS-Cu_2ZnSnS_4	$I\bar{4}$ (No. 82)	−4.596	−4.21[d]	…
ST-Cu_2ZnSnS_4	$I\bar{4}2m$ (No. 121)	−4.572	…	…
KS-Cu_2ZnSnO_4	$I\bar{4}$ (No. 82)	−9.275	…	…
ST-Cu_2ZnSnO_4	$I\bar{4}2m$ (No. 121)	−9.246	…	…

[a]Experiment from Ref. 53.
[b]Experiment from Ref. 54.
[c]Experiment from Ref. 55.
[d]Calculation from Ref. 26.
[e]Calculation from Ref. 27.

TABLE III. Summary of heats of formation results for CZTSe and related materials in units of eV per formula unit. For each formula unit given in the first column, the space-group symbol and number is listed in the second column. The heat formation ΔH is given in the third column, comparing the results of the present optimization study with literature and experimental values when available. In general, the detailed crystal structures corresponding to the experimental ΔH_{exp} are not known.

Formula unit	Crystal structure	ΔH
Se	$P2_1/c$ (No. 14)	−0.070,[a] −0.069[b]
CuSe	$Cmcm$ (No. 63)	−0.490,[a] −0.409,[b] −0.433[c]
CuSe	$P6_3/mmc$ (No. 194)	−0.466,[a] −0.30[d]
$CuSe_2$	$Pnnm$ (No. 58)	−0.617[a]
$CuSe_2$	$Pa\bar{3}$ (No. 205)	−0.615[a]
Cu_2Se	$F\bar{4}3m$ (No. 216)	−0.446[a]
Cu_2Se	$P4_32_12$ (No. 96)	−0.612[a]
Cu_2Se	$P2_1/c$ (No. 14)	−0.610,[a] −0.24,[d] −0.677[c]
Cu_3Se_2	$P\bar{4}2_1m$ (No. 113)	−1.422[a]
ZnSe	$F\bar{4}3m$ (No. 216)	−1.469,[a] −1.45,[d] −1.689[b] −1.691[c]
ZnSe	$P6_3mc$ (No. 186)	−1.463[a]
SnSe	$Pnma$ (No. 62)	−0.911[a]
SnSe	$Fm\bar{3}m$ (No. 225)	−0.901,[a] −0.90[d]
SnSe	$Cmcm$ (No. 63)	−0.899[a]
$SnSe_2$	$P\bar{3}m1$ (No. 164)	−1.032,[a] −1.04,[d] −1.105,[e] −1.29[c]
$CuSeO_3$	$P\bar{1}$ (No. 2)	−4.610[a]
$ZnSeO_3$	$Pbca$ (No. 61)	−6.869,[a] −6.761[c]
$Sn(SeO_3)_2$	$Pa\bar{3}$ (No. 205)	−11.679[a]
Cu_2SnSe_3	Cc (No. 9)	−2.116,[a] −1.80,[d] −1.760[e]
KS-$Cu_2ZnSnSe_4$	$I\bar{4}$ (No. 82)	−3.648,[a] −3.31,[d] −3.236[e]
ST-$Cu_2ZnSnSe_4$	$I\bar{4}2m$ (No. 121)	−3.621[a]

[a]Present work.
[b]Experiment from Ref. 53.
[c]Experiment from Ref. 55.
[d]Calculation from Ref. 28.
[e]Calculation from Ref. 21.

2. Comparison of present results to literature values of heats of formation

In constructing Tables II and III, we first modeled all the oxides of Cu, Zn, Sn, S, and Se for which heat of formation data is available in the CRC (Ref. 53) and NIST (Ref. 54) databases. We also modeled most of the non-metallic binary compounds of Cu, Zn, and Sn with O, S, and Se that were listed in the ICSD (Ref. 59) structural database. A few ternary non-metallic compounds were also considered. When possible we have noted the experimental heat of formation data for these materials, primarily from the CRC and NIST.[53,54] In addition, the Materials Thermochemistry text[55] lists heats of formation, which are generally identical to the CRC data except where noted separately in Tables II and III. The uncertainty of the experimental heat of formation data listed in Ref. 55 is mostly less than 0.02 eV/atom with a few exceptions such as ZnSe and Sn_2S_3, which have uncertainties of 0.05 and 0.04 eV/atom, respectively.

Of the compounds used to set the "standard" energy for elemental O (indicated with an "*" in Table II), the deviation between the simulations and experiment is typically 0.2 eV/formula unit or less with the exception of SO_3, where the deviation is 0.4 eV/formula unit. Interestingly, the related sulfate materials $CuSO_4$ and $ZnSO_4$ have calculated heats of formation in agreement with the average experimental results within 0.1 eV/formula unit. The detailed comparison between the calculations and experiment is made more difficult by the fact that structural information is rarely recorded for the experimental heat of formation data. On the other hand, the calculated lowest energy heats of formation are typically in good agreement with the experimental results[53–55] and previous calculations.[21,26,27,60] The largest differences between our results and previous calculations[26] occur for Cu_2S and Cu_2Se, where our results indicate larger magnitudes for heats of formation, in better agreement with experimental values.

Even though it is beyond the scope of the present work, to make a complete survey of all compounds of Cu, Zn, Sn, S, Se, and O, the results presented in Tables II and III show some interesting trends. For example, we find the ground state structures of CuS and CuSe to have $Cmcm$ symmetry. Low temperature structural studies of these materials find this structure to be only stable at low temperature (around 55 K).[61] For CuS_2, the ground state structure has the symmetry $Pa\bar{3}$, while the corresponding $CuSe_2$ material has slightly higher energy than the $Pnnm$ structure. For Cu_2S, of the two structures we considered, the lower energy structure has $P2_1/c$ symmetry, while crystals in the $P4_32_12$ structure have 0.008 eV higher energy. We did not consider the more complicated cubic structures of this compound.[62] For the corresponding Cu_2Se materials, the ground state structure is computed to have $P4_32_12$ symmetry and the $P2_1/c$ structure is computed to have nearly the same energy (0.002 eV higher). In fact, the $P4_32_12$ structure for Cu_2Se, based on the Cu_2S analog, is not reported in ICSD,[59] while our calculations suggest that it is at least meta-stable.

3. Predictions of relative stability and possible reactions

From the values of the heats of formation shown in Tables II and III, it is possible to predict synthesis and decomposition processes for the CZTS family. Table IV lists some of the possible synthesis processes for CZTS, CZTSe, and CZTO. In calculating the reaction energies ΔH^R_{cal}, the lowest calculated energy structures given in Tables II and III were used except for CuS, CuSe, and Cu_2Se. For CuS and

TABLE IV. Possible synthesis reactions for the CZTS family of compounds based on Tables II and III. All values of ΔH^R_{cal} are given in units of eV/reaction.

Starting materials	Product	ΔH^R_{cal}
$Cu_2S + ZnS + SnS_2$	Cu_2ZnSnS_4	−0.573
$2CuS + ZnS + SnS$	Cu_2ZnSnS_4	−0.326
$Cu_2SnS_3 + ZnS$	Cu_2ZnSnS_4	−0.142
$Cu_2Se + ZnSe + SnSe_2$	$Cu_2ZnSnSe_4$	−0.536
$2CuSe + ZnSe + SnSe$	$Cu_2ZnSnSe_4$	−0.288
$Cu_2SnSe_3 + ZnSe$	$Cu_2ZnSnSe_4$	−0.063
$Cu_2O + ZnO + SnO_2$	Cu_2ZnSnO_4	1.679
$2CuO + ZnO + SnO$	Cu_2ZnSnO_4	0.374
$Cu_2SnO_3 + ZnO$	Cu_2ZnSnO_4	0.073

CuSe, the hexagonal $P6_3/mmc$ form was chosen and for Cu_2Se, the $P2_1/c$ structure was used.

Although the ground state simulations give no information about possible reaction barriers, the values of ΔH^R_{cal} estimate the net heat released ($\Delta H^R_{cal} < 0$) or absorbed ($\Delta H^R_{cal} > 0$) in the reaction. This suggests that exothermic reactions ($\Delta H^R_{cal} < 0$) are more likely to occur than the endothermic reactions. Here, Table IV indicates that CZTS can be synthesized through solid state reaction techniques using Cu_2S, ZnS, SnS_2, or CuS, ZnS, SnS, or ZnS, Cu_2SnS_3 as starting materials. Actually, these synthesis reactions were studied by Schorr *et al.*[63] using *in-situ* X-ray analysis and all three reactions were successful in producing KS-CZTS. Our results shown in Table IV predict that CZTSe will behave in a similar manner.

By contrast, the positive value of ΔH^R_{cal} for CZTO listed in Table IV, implies that solid state synthesis methods using binary or ternary oxide starting materials would require significant heating. The fabrication of pure CZTO has been reported,[13] by means of an open atmosphere type chemical vapor deposition procedure using the mixture of reactant vapors $Cu(C_5H_7O_2)_2$, $Zn(C_5H_7O_2)_2$, and $Sn(C_5H_7O_2)_2$. In fact, the large positive value of ΔH^R_{cal} implies that CZTO is not stable relative to its binary constituents. However, the observation of pure CZTO by Washio *et al.*[13] and others, is consistent with our simulations of ideal metastable crystals of the material.

Besides the studying of stoichiometric CZTS family, the effects of excess Cu, Zn, or Sn on the reactions were explored, as listed in Table V. All the exothermic reactions shown in Table V reveal that decomposition of CZTS and CZTSe could be triggered in the presence of excess Cu, Zn, or Sn, with the largest exothermic effect occurring for Zn. Some of these reactions have been investigated in the study of thin film growth using controlled layers of metallic precursors.[64]

Moreover, several authors[18,26,28,65] have considered heats of formation data such as that given in Tables II and III to determine the phase stability of CZTS and CZTSe in terms of the elemental chemical potentials μ_{Cu}, μ_{Zn}, μ_{Sn}, μ_S, and μ_{Se}. Here, the chemical potentials are referenced to the standard elemental states as described in Sec. III B. From a number of constraints and inequalities, it is possible to estimate the "volume" in chemical potential space representing the region of pure CZTS or CZTSe. For example, the constraints and inequalities for CZTS are

TABLE V. Possible decomposition reactions for the CZTS family of compounds based on Tables II and III. All values of ΔH^R_{cal} are given in units of eV/reaction.

Starting materials	Product	ΔH^R_{cal}
$Cu_2ZnSnS_4 + 2Cu$	$2Cu_2S + ZnS + SnS$	−0.112
$Cu_2ZnSnS_4 + Zn$	$Cu_2S + 2ZnS + SnS$	−0.955
$Cu_2ZnSnS_4 + Sn$	$Cu_2S + ZnS + 2SnS$	−0.253
$Cu_2ZnSnSe_4 + 2Cu$	$2Cu_2Se + ZnSe + SnSe$	−0.048
$Cu_2ZnSnSe_4 + Zn$	$Cu_2Se + 2ZnSe + SnSe$	−0.811
$Cu_2ZnSnSe_4 + Sn$	$Cu_2Se + ZnSe + 2SnSe$	−0.253

$$\begin{aligned}
2\mu_{Cu} + \mu_{Zn} + \mu_{Sn} + 4\mu_S &= \Delta H_{cal}(CZTS)\\
\mu_{Cu} + \mu_S &< \Delta H_{cal}(CuS)\\
2\mu_{Cu} + \mu_S &< \Delta H_{cal}(Cu_2S)\\
\mu_{Zn} + \mu_S &< \Delta H_{cal}(ZnS)\\
\mu_{Sn} + 2\mu_S &< \Delta H_{cal}(SnS_2)\\
2\mu_{Cu} + \mu_{Sn} + 3\mu_S &< \Delta H_{cal}(Cu_2SnS_3)\\
\mu_{Cu} &< 0\\
\mu_{Zn} &< 0\\
\mu_{Sn} &< 0\\
\mu_S &< 0.
\end{aligned} \tag{1}$$

It is convenient to assume that μ_S is determined in terms of the other chemical potentials by the constraint relation in Eq. (1). Then, the full constraint and inequality relations of Eq. (1) determine a volume in μ_{Cu}, μ_{Zn}, and μ_{Sn} chemical potential space, which represents the region where CZTS is stable compared with formation of binary and ternary compounds of Cu, Zn, Sn, and S. A visualization of the volumetric stability region is presented in Appendix A. This thermodynamic stability analysis suggests that the main secondary impure phases that limit the formation of pure CZTS are ZnS, CuS, SnS, and Cu_2SnS_3, which is in agreement with the work of Walsh *et al.*[26] To see these results more clearly, we can project the results onto the μ_{Cu} axis as shown in Fig. 1. The figure also includes results for CZTSe analyzed in the same way. It is worth mentioning that Cu_3Se_2 could affect the stability volume of CZTSe, however, under typical synthesis conditions, the temperatures higher than 315 °C are used so that Cu_3Se_2 transforms to Cu_2Se.[66] Therefore, the effect of Cu_3Se_2 is ignored here. From Fig. 1, it is apparent that the existence region of single phase CZTSe is smaller than that of CZTS, suggesting that the synthesis of pure CZTSe is more difficult than pure CZTS. Interestingly, a similar phase analysis for CZTO finds no regions of stability. This further suggests the difficulty of producing CZTO with the use of binary and ternary oxides of Cu, Zn, and Sn.

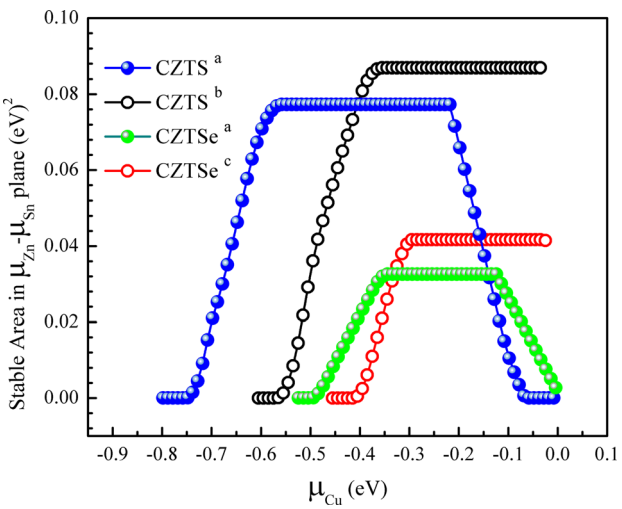

FIG. 1. Plot of μ_{Cu} versus area in the μ_{Zn}-μ_{Sn} plane defining the regions of stability of CZTS and CZTSe, comparing the results of the present work (a) to those of Refs. 26 (b) and 28 (c).

Because of the slightly different heats of formation calculated in our results (particularly for Cu_2S and Cu_2Se) compared with that reported in Refs. 26 and 28, the computed stability volumes in chemical potential space are not identical as shown in Figs. 1 and 9 of Appendix A. We see that the difference between our results with that of the previous literature mainly occurs for μ_{Cu} close to zero, which corresponds to Cu in its elemental ground state.

The significance of plot in Fig. 1 is that, for values of μ_{Cu} with non-zero stability areas, it is expected that the formation of pure CZTS or CZTSe is possible. Unfortunately, apart from correlating $\mu_{Cu}=0$ with Cu in its elemental ground state, it is difficult to directly know and control the value of μ_{Cu}. However, we can say that the values of μ_{Cu} corresponding compounds of Cu and S or Se listed in Table IV represent values *inside* the stability region, while μ_{Cu} corresponding to the combination of elemental Cu and compounds of Cu and S or Se listed in Table V represent values *outside* the stability region.

C. Simulations of oxidation and selenization of CZTS

In order to perform the alloy simulations, supercell techniques were used. The main "supercell" considered was the conventional unit cell containing 16 atoms including 8 equivalent S positions. For these calculations, the **k**-point sampling of $8\times8\times4$ was used. The energy convergence was checked with equivalent calculations using the primitive cells containing 8 atoms, and supercells containing 64 and 128 atoms. For the conventional and supercell simulations, the lattice optimizations were constrained to maintain orthorhombic symmetry, but the *a* and *b* lattice parameters were allowed to differ. The calculated energy difference between equivalent primitive and conventional cell results is less than 0.006 eV/formula unit. Between equivalent 16 atom conventional cell and 128 atom supercell results, the difference is less than 0.002 eV/formula unit.

For the study of the $Cu_2ZnSnS_xO_{4-x}$ and $Cu_2ZnSnS_xSe_{4-x}$ alloy systems, we focussed our attention on the kesterite ($I\bar{4}$) structure and assumed the kesterite arrangements of the Cu, Zn, and Sn sites, with substitutions on the S sites. A systematic approach was used in order to scan the possible alloy configurations of the system within the conventional unit cell, using translation and point group symmetries to find the unique configurations. Similar methods for studying disordered systems have been described in the literature.[67] In our systems, there are eight sulfur sites in the conventional unit cell substituted by $2x$ alloy atoms with a total of $2^8=256$ configurations. For the given values of $x=0$, 0.5, 1, 1.5, 2, 2.5, 3, 3.5, 4, the number of configurations are given by the binomial coefficients $\binom{8}{2x}=1,8,28,56,70,56,28,8,1$, respectively. However, because the eight sulfur sites (8g in the Wyckoff designation[45]) are related by 8 space group symmetries in addition to the crystal periodicity, the number of physically unique configurations is considerably fewer. For example, four equivalent configurations of $Cu_2ZnSnS_xO_{4-x}$ are illustrated for $x=2$ in Fig. 2; the equivalence of these configurations is due to translations of the simulation cell along the **c** axis. Using the full symmetry analysis for these systems, the number of unique alloy configurations for this system is reduced to 1, 1, 5, 5, 10, 5, 5, 1, 1 for the 9 values of x. The numerical accuracy of the symmetry equivalence was checked for a number of cases, finding errors smaller than 0.001 eV/atom.

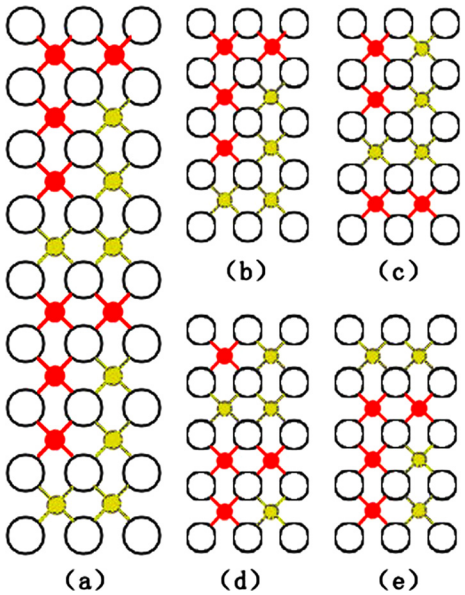

FIG. 2. Schematic representation of some equivalent configurations for a $Cu_2ZnSnS_2O_2$ alloy. The open circles represent the fixed positions of the Cu, Zn, and Sn ions, while the dark (red) and light (yellow) filled circles represent S or O positions. The vertical direction of the figure shows the c axis of the crystal, while the a and b are schematically shown along the horizontal direction of the drawing. Drawing (a) shows two unit cells of a particular configuration, periodically repeated along the c axis. Drawings ((b)–(e)) show single unit cells of equivalent configurations generated by origin shifts along the c axis.

1. Energies and lattice parameters of optimized alloy configurations

The results of the alloy optimizations are summarized in Appendix B in Table VI for the CZTSO systems and in Table VII for the CZTSSe systems. From these tables, it is apparent that O causes significant tetrahedral distortion with $|a_i-b_i|$ values as large as 0.2 Å. In addition, for some values of x (such as $x=2$), there is a significant range of the formation energies, with $\Delta H_i(x)$ values differing by as much as 0.2 eV. [To simplify the notation in this section, the subscript "*cal*" is omitted.] By contrast, for the Se alloys, the lattice distortion and variation in the heats of formation are 10 times smaller.

In order to relate the computed alloy sampling to experimental measurements, it is necessary to evaluate appropriate average quantities. For our simulations, statistical mechanical considerations based on the temperature of the material and the Boltzmann distribution are used to determine the probability factor $p_i(x)$ for each unique simulation configuration i. The average value of a quantity $v_i(x)$ (such as lattice parameter, heat of formation, etc.) can then be computed from an expression of the form

$$\langle v(x)\rangle_T = \sum_i p_i(x)v_i(x), \quad \text{where}$$
$$p_i(x) = \frac{g_i e^{-\Delta H_i(x)/kT}}{\sum_j g_j e^{-\Delta H_j(x)/kT}}. \tag{2}$$

In Eq. (2), the summations over i and j include all unique configurations consistent with the given value of x. The notation g_i represents the multiplicity factor, k denotes the Boltzmann constant, and T denotes the temperature in degrees K.

Because of the significant range in the heats of formation for the CZTSO alloys, the average quantities show a non-trivial temperature dependence compared with those of the CZTSSe alloys. When appropriate, we evaluated the averages for temperatures $T = 300$ K, 800 K, and ∞.

Figure 3 shows the calculated optimized lattice parameters $(a+b)/2$ and c as a function of S concentration for kesterite-based CZTSO alloys. For a given value of x, the range of the lattice parameters for the various alloy configurations is considerable, particularly for $x = 2$. Interestingly, the range of the energies ΔH_i for these configurations as shown in Table VI are considerably larger than kT, so that the average lattice parameters at $T = 300$ K are measurably different from those at $T = \infty$.

Both experimental[68,69] and computational[24,25] work on the CZTSSe alloy system have been reported. The results of the present study are shown in Fig. 4 in terms of the weighted average of $(a+b)/2$ and c for each unique alloy configuration. In this case, the range of ΔH_i is small enough that there is negligible temperature effect on the averaging. Within the expected 2% underestimation of the lattice constants, the calculated results agree well with the experimentally measured values[68,69] indicated on the plot. Our calculated results are also in good agreement with the simulations of Camps *et al.*,[25] who used similar computational methods with 64 atom supercells and random sampling techniques to investigate alloy configurations.

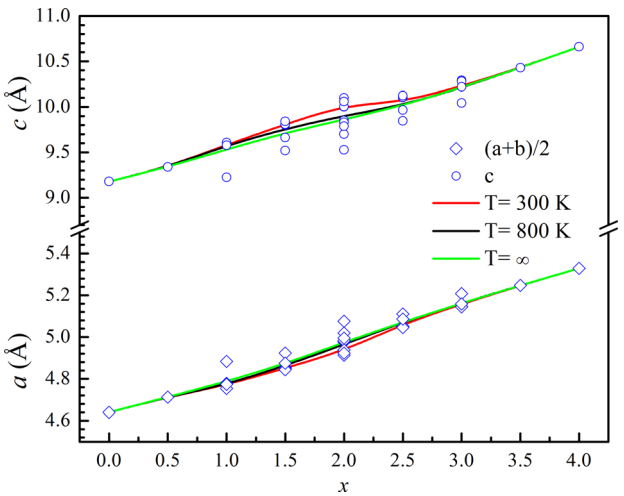

FIG. 3. The calculated lattice parameters $(a+b)/2$ and c as a function of x indicating the concentration of sulfur for $Cu_2ZnSnS_xO_{4-x}$. The solid lines indicate the average values evaluated using Eq. (2) for temperatures $T = 300$ K, 800 K, and ∞. The separate symbols indicate the individual values, each unique configuration i in the simulation.

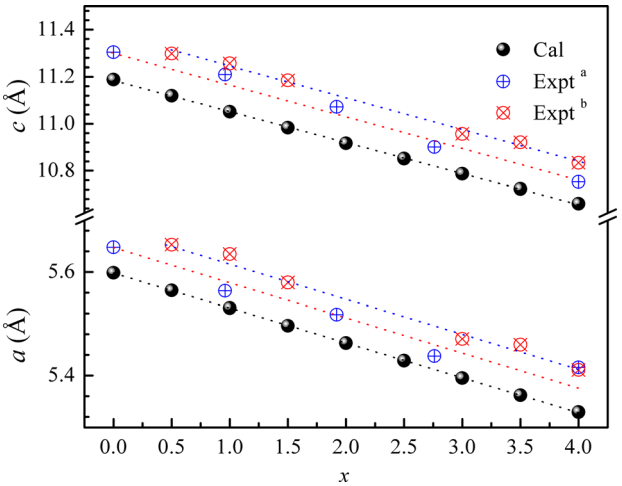

FIG. 4. The calculated lattice parameters $(a+b)/2$ and c as a function of x indicating the concentration of sulfur for kesterite-based CZTSSe alloys compared with experimental data from Refs. 68 (a) and 69 (b).

The energy analysis results can be used to estimate various alloy reactions. One possible method of forming the alloy systems is through substitution reactions, which for the CZTSO system takes the form

$$R1: Cu_2ZnSnS_4 + (4-x)\frac{1}{2}O_2 \rightarrow Cu_2ZnSnS_xO_{4-x} + (4-x)S. \tag{3}$$

We considered this reaction in several different ways. First, the substituting elements (S and O) were assumed to participate in their ground states. For the CZTSO system, the corresponding net reaction energy denoted $\Delta H^{R1}(x)$ can be estimated from the difference in the heats of formation $\Delta H^{R1}(x) \approx \Delta H(Cu_2ZnSnS_xO_{4-x}) - \Delta H(Cu_2ZnSnS_4)$. A more physical estimate of the relevant substitution reaction for the CZTSO alloys might involve the formation of SO_2 gas

$$R2: Cu_2ZnSnS_4 + (4-x)(1+\frac{1}{2})O_2 \rightarrow Cu_2ZnSnS_xO_{4-x} + (4-x)SO_2. \tag{4}$$

The reaction energy $\Delta H^{R2}(x)$ for Eq. (4) can be estimated using $\Delta H^{R2}(x) \approx \Delta H^{R1}(x) + \Delta H(SO_2)$, where $\Delta H(SO_2)$ denotes the heat of formation of the SO_2 gas, which is experimentally measured to be −3.08 eV according to Ref. 55.

For the CZTSSe system, the substitution reaction is given by

$$R3: Cu_2ZnSnS_4 + (4-x)Se \rightarrow Cu_2ZnSnS_xSe_{4-x} + (4-x)S. \tag{5}$$

The net reaction energy $\Delta H^{R3}(x)$ can be estimated from the difference in the heats of formation $\Delta H^{R3}(x) \approx \Delta H(Cu_2ZnSnS_xSe_{4-x}) - \Delta H(Cu_2ZnSnS_4)$. Instead of S and Se in their ground states, the reaction energy of this system denoted by $\Delta H^{R4}(x)$ for the high temperature formation of CZTSSe alloys should include the atomization energies for S and Se. The experimental values of atomization energies for

S and Se are 2.87 eV and 2.44 eV, respectively.[55] An even more physical estimate of the reaction might involve the formation of S_n and Se_n $(0 \le n \le 8)$ molecules in gaseous form, which could significantly lower the reaction energy. This more complicated reaction system needs further consideration.

The averaged reaction energies for $R1$, $R2$, $R3$, and $R4$ are plotted as a function of the S concentration parameter x in Fig. 5. Interestingly, the two estimates of the reactions involving oxygen substituting for S (ΔH^{R1} and ΔH^{R2}) are predicted to be very exothermic. This suggests that with exposure to oxygen, the incorporation of oxygen in the CZTS lattice is very likely to occur. Figure 5 also explains the results of Washio *et al.*, who reported that in order to produce CZTSO by sulfurization of CZTO, it is necessary to use temperatures as high as 520–560 °C and reaction times of approximately 3 h. On the other hand, the reactions involving Se substituting for S (ΔH^{R3} and ΔH^{R4}) are predicted to be endothermic, indicating that selenization of pure CZTS can only be accomplished with high temperature, which has been shown in experiment.[2,70] Therefore, from Figs. 1 and 5, our analysis suggests that it is easier to synthesize pure CZTS than CZTSe, while the formation of the alloy CZTSSe is more easily accomplished by the sulfurization of CZTSe than by the selenization of CZTS.

Another aspect of the results is the analysis of the alloy formation reactions analogous to those discussed for the pure materials in Table IV. In this case, we consider the most exothermic reactions from Table IV for possible synthesis of CZTSO and CZTSSe alloys.

$$R5: \frac{x}{4}(Cu_2S + ZnS + SnS_2) + \left(1 - \frac{x}{4}\right)(Cu_2O + ZnO + SnO_2) \rightarrow Cu_2ZnSnS_xO_{4-x}, \quad (6)$$

$$R6: \frac{x}{4}(Cu_2S + ZnS + SnS_2) + \left(1 - \frac{x}{4}\right)(Cu_2Se + ZnSe + SnSe_2) \rightarrow Cu_2ZnSnS_xSe_{4-x}. \quad (7)$$

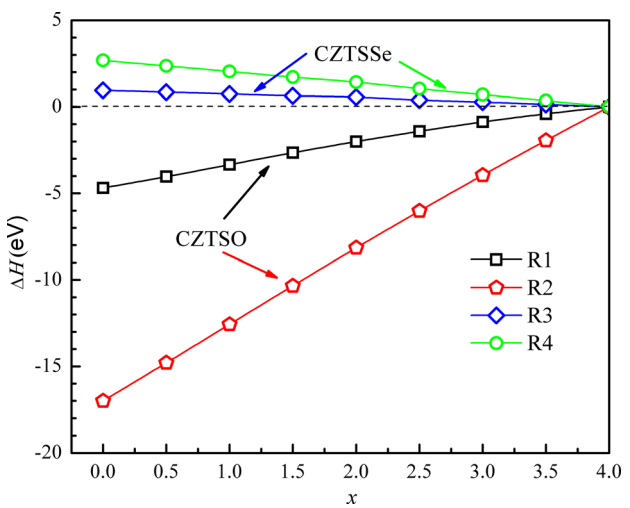

FIG. 5. Calculated reaction energies $\Delta H^{R1}(x)$, $\Delta H^{R2}(x)$, $\Delta H^{R2}(x)$, and $\Delta H^{R4}(x)$ averaged over all alloy configurations and plotted as a functions of x.

Using the sign convention presented in Sec. III B 3, negative values of the net reaction energies imply that the crystalline alloy is more stable than its binary constituents, while positive values imply the opposite. A plot of $\Delta H^{R5}(x)$ and $\Delta H^{R6}(x)$ is given in Fig. 6. We see that the $Cu_2ZnSnS_xSe_{4-x}$ alloys are computed to be stable throughout the full range of x. These results suggest that reaction $R6$ may be a useful method of producing CZTSSe alloys, allowing better control of the S/Se ratio than reaction $R3$. On the other hand, the $Cu_2ZnSnS_xO_{4-x}$ alloys are computed to be unstable with respect to decomposition into the binary oxides and sulfides for $0 \le x \le 3.3$. There is not very much quantitative evidence of CZTSO or its decomposition products reported in the literature. However, Schurr *et al.*[71] observed X-ray diffraction patterns of CuO and SnO_2 in some of their synthesized samples of CZTS.

2. Analysis of alloy configurations

In principle, the simulations are able to balance the competing physical effects such as atomic hybridization, crystal field splitting, polarization of charge, lattice strains, etc., in order to determine the lowest energy structures. Examination of the optimized geometries resulting from the calculations can provide information on which of the physical effects are important for our system. Figure 7 shows three of the configurations of the $x = 2$ case. The lowest energy structure has alternating S and O sites in the a–b planes, while the highest energy structures have a–b planes of S sites and others of O sites. It is apparent that the alternation of short and long bonds to the Cu, Zn, and Sn ions causes significant distortion from ideal tetrahedral bonding. The energy difference between the lowest energy configuration (Fig. 7(b)) and highest energy configuration (Fig. 7(d)) is 0.2 eV. Also shown (Fig. 7(c)) is an intermediate energy configuration, which maintains the tetragonal symmetry of the lattice ($a_i = b_i$) and accommodates some layers of pure MS_4 tetrahedra and others of pure MO_4 tetrahedra for M = Cu and Sn.

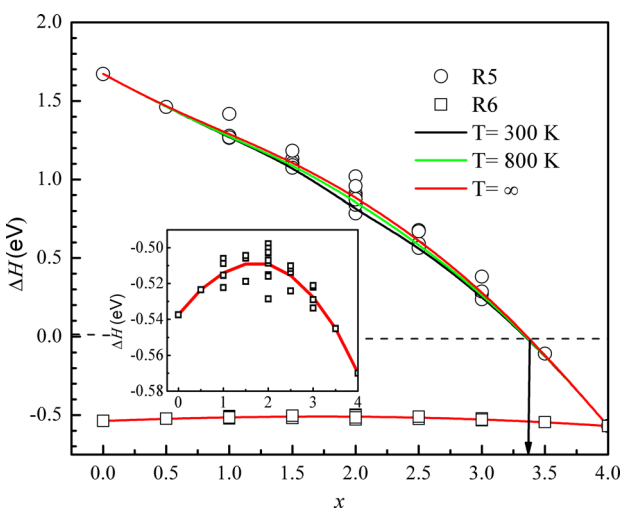

FIG. 6. Reaction energies for formation of CZTSO (reaction $R5$) and formation of CZTSSe (reaction $R6$). Solid line shows weighted averages of unique configuration results, which are also indicated using separate symbols. Insert shows energies for $R6$ on an expanded scale.

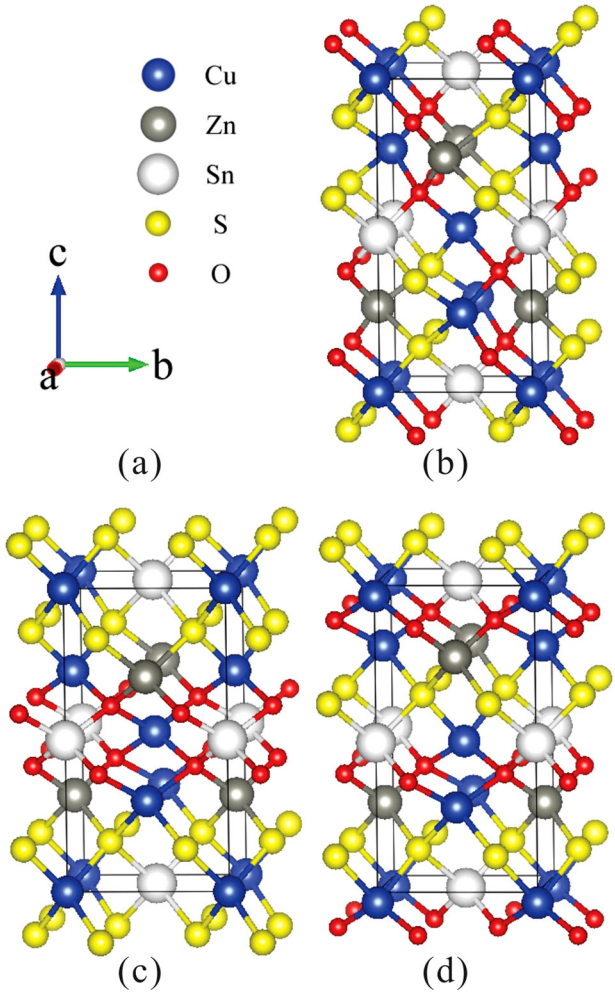

FIG. 7. Ball and stick diagram of the primitive simulation cell for CZTSO alloys with $x = 2$ showing 3 of the 10 unique configurations. (a) Ball convention and the orientation of the simulation cell. (b) Structure of lowest energy configuration with $\Delta H_i = -6.70$ eV. (c) A high symmetry configuration with $\Delta H_i = -6.58$ eV. (d) Structure of the highest energy configuration with $\Delta H_i = -6.47$ eV.

Figure 8 shows the lowest and highest energy configurations of the $x = 1.5$ case. The highest energy structure in this case shares structural similarity with that of the $x = 2$ case in that both are characterized with the segregation of S and O in different *a*–*b* layers. The energy difference between the highest and lowest energy structures of the $x = 1.5$ system is 0.1 eV.

For the CZTSSe alloys, our results show the optimal geometries to be very similar to those of the CZTSO alloys, although the tetrahedral bond distortions are much smaller. Correspondingly, the energy difference between the highest and lowest energy configurations of the CZTSSe alloys is smaller by a factor of 1/8 or less compared with the CZTSO alloys. While the energy range of CZTSSe configurations is small and, in some cases, within the calculational error, the results show a correspondence with the configurations found in the CZTSO simulations. For $x = 2$, for example, the lowest and highest energy CZTSSe configurations are similar to the geometries shown in Figs. 7(b) and 7(d), respectively. These results are consistent with the work of Khare *et al.*,[24] who performed similar simulations based on primitive cell lattices of CZTSSe alloys. These authors used the convenient

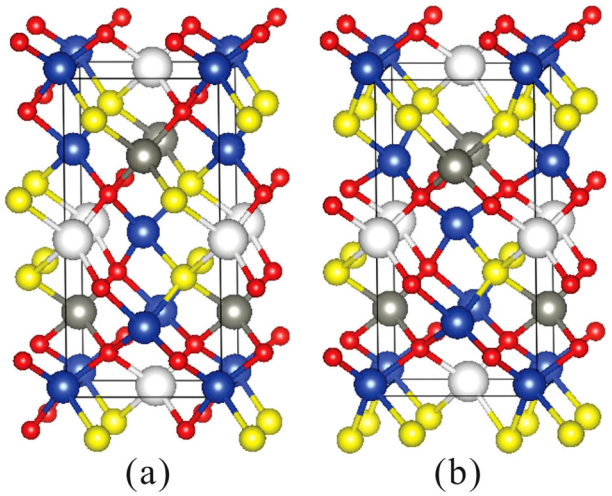

FIG. 8. Ball and stick diagram of primitive simulation cell configurations of CZTSO system with $x = 1.5$ showing 2 of the 5 unique configurations using the same conventions as Fig. 7. (a) Structure of the lowest energy configuration with $\Delta H_i = -7.28$ eV. (b) Structure of the highest energy configuration with $\Delta H_i = -7.17$ eV.

nomenclature of "uniform" distribution for the configuration of Fig. 7(b) and "layered" distribution of Fig. 7(d). While the simulations determine the energetic preference of the "uniform" distribution of Se substitutions in the CZTSSe alloys, the fact that for a given value of x, the energy range between configurations is within kT. This suggests that under experimental conditions, the CZTSSe alloys are likely to formed with equal likelihood of each microscopic configuration, resulting in a homogeneous distribution of Se in the macroscopic systems.

IV. SUMMARY AND CONCLUSIONS

In this work, we have explored the detailed properties of kesterite structures of Cu_2ZnSnO_4 and of the alloy system $Cu_2ZnSnS_xO_{4-x}$. Together with a brief study of the corresponding stannite structures and a parallel study of Cu_2ZnSnS_4 and of the alloy system $Cu_2ZnSnS_xSe_{4-x}$, we can draw the following conclusions:

(1) Using a variety of supercells, our computer simulations show that Cu_2ZnSnO_4 and of the alloy system $Cu_2ZnSnS_xO_{4-x}$ have well-defined structures, which are stable or at least meta-stable. A systematic scan of possible alloy configurations for each given value of x in the $Cu_2ZnSnS_xO_{4-x}$ alloys shows a significant range in predicted lattice constants (0.1 Å for a and 0.2 Å for c) and in their corresponding heats of formation (0.2 eV).
(2) In considering the heats of formation of the $Cu_2ZnSnS_xO_{4-x}$ alloys in comparison with respect pure Cu_2ZnSnS_4, we find that with exposure to oxygen, oxygen incorporation in the CZTS lattice is very likely to occur.
(3) In considering the heats of formation of the $Cu_2ZnSnS_xO_{4-x}$ alloys in relationship with binary or ternary oxides and sulfides, we find that the alloys are only stable with respect to decomposition into the binary oxides and sulfides for the small range of $3.3 < x < 4.0$.

(4) We have studied possible synthesis reactions for CZTS and CZTSe as listed in Table IV, finding that solid state reactions using binary and ternary sulfides and selenides can form CZTS and CZTSe with a net release of energy. We also studied possible decomposition reactions of CZTS and CZTSe as listed in Table V, finding that excess Cu, Zn, or Sn can cause decomposition into binary compounds, with Zn releasing the largest energy.
(5) For the CZTSSe alloys, the range of heats of formation $\Delta H_i(x)$ was found to be 0.04 eV or less, suggesting that at room temperature, the alloys have random distributions of Se substitutions on S sites. By contrast, the CZTSO alloys have preferred configurations in which O sites are not concentrated in any *a–b* plane as shown in Fig. 7.
(6) For the synthesis of CZTSSe alloys, the heat of formation results and reaction *R*3 show that it is energetically more favorable to sulfurize CZTSe than to selenize CZTS. On the other hand, the phase diagram results shown in Fig. 1 indicate that it is easier to synthesize CZTS than CZTSe.

With the computational result which predicts that oxygen incorporation in the CZTS lattice is very likely to occur, it is interesting that direct experimental evidence of crystalline CZTSO alloys has not appeared in the literature (such as the identification of distinct X-ray patterns). Whether this is because the X-ray patterns might be very broad due to the large range of structural forms for each stoichiometry, or whether the CZTSO alloys are likely to decompose into the binary and ternary oxides and sulfides, producing even more broad X-ray patterns, remain a question for further work.

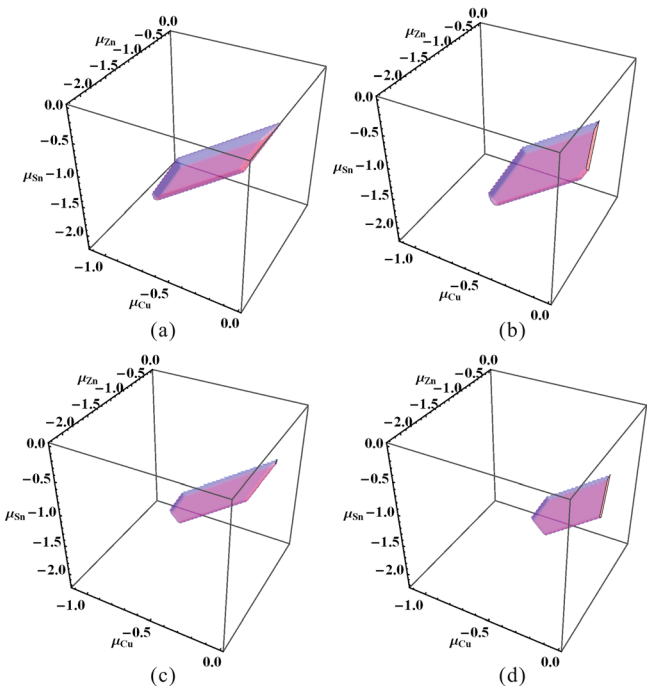

FIG. 9. Mathematica visualization of the volumes in μ_{Cu}, μ_{Zn}, μ_{Sn} chemical potential space, which satisfies the constraints and inequalities of Eq. (1). Volumes (a) for CZTS and (c) for CZTSe were constructed from values of ΔH_{cal} determined in this work (Tables II and III). Volumes (b) for CZTS and (d) for CZTSe were constructed from values of ΔH_{cal} determined from Refs. 26 and 28.

Together with the recent experimental studies of oxygen in the CZTS system by Washio *et al.*,[13] our work encourages additional study of the CZTSO system.

ACKNOWLEDGMENTS

This work was supported by NSF Grant No. DMR-115485. Helpful discussions with Qi Li, Zachary Hood, Abdou Lachgar, and Cynthia Day are gratefully acknowledged.

APPENDIX A: DETAILS OF CHEMICAL POTENTIAL STABILITY ANALYSIS

In Sec. III B 3, we discussed the range of phase stability of CZTS and CZTSe in terms of the elemental chemical potentials following the work of previous authors.[18,26,28,65] This type of analysis provides information about the

TABLE VI. Calculated lattice parameters and heats of formation for KS-$Cu_2ZnSnS_xO_{4-x}$ alloys for each value of x and unique configuration i. The number of equivalent configurations g_i (of the 256 total) is listed in the second column. The heat of formation $\Delta H_i(x)$ (in eV/formula unit) is listed in the column of three. The optimized lattice constants (a_i, b_i, and c_i (Å units) are given in various combinations in the last three columns.

x	g_i	ΔH_i	$(a_i+b_i)/2$	$\lvert a_i-b_i\rvert$	$c_i/(a_i+b_i)$
0.0	1	−9.28	4.64	0.00	0.989
0.5	8	−8.63	4.71	0.14	0.991
1.0	4	−7.80	4.88	0.21	0.945
1.0	4	−7.94	4.78	0.09	1.002
1.0	8	−7.95	4.77	0.07	1.003
1.0	8	−7.95	4.77	0.07	1.003
1.0	4	−7.96	4.75	0.08	1.010
1.5	8	−7.17	4.87	0.04	0.991
1.5	16	−7.22	4.92	0.01	0.967
1.5	8	−7.25	4.85	0.04	1.010
1.5	8	−7.26	4.85	0.10	1.012
1.5	16	−7.28	4.84	0.10	1.016
2.0	2	−6.47	5.02	0.07	0.966
2.0	2	−6.53	4.94	0.23	1.013
2.0	2	−6.53	4.94	0.23	1.013
2.0	16	−6.58	4.98	0.03	0.989
2.0	4	−6.58	5.08	0.00	0.938
2.0	16	−6.59	4.98	0.07	0.988
2.0	8	−6.60	4.98	0.03	0.987
2.0	8	−6.61	4.92	0.02	1.022
2.0	8	−6.65	4.99	0.08	0.980
2.0	4	−6.70	4.91	0.02	1.028
2.5	8	−5.94	5.05	0.09	1.001
2.5	8	−5.94	5.05	0.15	1.000
2.5	8	−5.95	5.09	0.02	0.980
2.5	16	−6.03	5.11	0.05	0.963
2.5	16	−6.06	5.05	0.01	1.003
3.0	4	−5.37	5.15	0.01	1.000
3.0	8	−5.47	5.16	0.07	0.991
3.0	8	−5.47	5.16	0.07	0.990
3.0	4	−5.48	5.21	0.03	0.964
3.0	4	−5.52	5.14	0.01	0.999
3.5	8	−5.00	5.25	0.00	0.994
4.0	1	−4.59	5.33	0.00	1.000

synthesis of pure CZTS and CZTSe in competition with secondary phases of binary and ternary compounds. Figure 9 was constructed using Mathematica and the set of constraints and inequalities given in Eq. (1) to visualize the stable volumes of the quaternary compounds in chemical potential space. From this volumetric analysis, we constructed Figure 1 by calculating cross-sectional areas in chemical potential space along the μ_{Cu} axis. Because the analysis is sensitive to small differences in the calculated heats of formation, the resulting volumes of stability for CZTS and CZTSe determined in the present work is slightly different from that of the previous work,[26,28] especially when μ_{Cu} is close to zero.

APPENDIX B: DETAILS OF CZTSO AND CZTSSE ALLOY RESULTS

The tables below list the optimized lattice parameters and heats of formation for the $Cu_2ZnSnS_xO_{4-x}$ and $Cu_2ZnSnS_xSe_{4-x}$ discussed in Sec. III C 1. For each value of x, the results are listed in order of increasing values of ΔH^i_{cal}.

TABLE VII. Lattice parameters and energies for KS-$Cu_2ZnSnS_xSe_{4-x}$ alloys for each value of x and unique configuration i using the same columns and units as in Table VI.

x	g_i	ΔH_i	$(a_i+b_i)/2$	$\lvert a_i-b_i\rvert$	$c_i/(a_i+b_i)$
0.0	1	−3.65	5.60	0.00	0.999
0.5	8	−3.75	5.56	0.00	0.999
1.0	4	−3.84	5.53	0.00	1.000
1.0	4	−3.85	5.53	0.00	0.999
1.0	8	−3.85	5.53	0.00	0.999
1.0	8	−3.85	5.53	0.00	0.999
1.0	4	−3.86	5.53	0.00	1.000
1.5	8	−3.96	5.49	0.00	1.000
1.5	16	−3.96	5.50	0.00	0.999
1.5	8	−3.96	5.50	0.01	0.999
1.5	8	−3.96	5.50	0.00	0.999
1.5	16	−3.97	5.50	0.00	0.999
2.0	4	−4.06	5.46	0.00	0.999
2.0	2	−4.07	5.46	0.00	1.001
2.0	2	−4.07	5.46	0.01	0.998
2.0	2	−4.07	5.46	0.01	0.998
2.0	8	−4.07	5.46	0.00	0.999
2.0	16	−4.07	5.46	0.00	0.999
2.0	16	−4.08	5.46	0.00	0.999
2.0	8	−4.08	5.46	0.00	0.999
2.0	8	−4.08	5.46	0.00	0.999
2.0	4	−4.10	5.46	0.00	1.000
2.5	8	−4.19	5.43	0.00	1.000
2.5	8	−4.19	5.43	0.01	0.999
2.5	8	−4.19	5.43	0.00	0.999
2.5	16	−4.19	5.43	0.00	0.999
2.5	16	−4.20	5.43	0.00	1.000
3.0	4	−4.32	5.40	0.00	1.000
3.0	4	−4.32	5.40	0.00	1.000
3.0	8	−4.32	5.40	0.00	1.000
3.0	8	−4.32	5.40	0.00	0.999
3.0	4	−4.33	5.39	0.00	1.001
3.5	8	−4.45	5.36	0.00	1.000
4.0	1	−4.59	5.33	0.00	1.000

[1]Y. Cao, M. S. Denny, J. V. Caspar, W. E. Farneth, Q. Guo, A. S. Ionkin, L. K. Johnson, M. Lu, I. Malajovich, D. Radu, H. D. Rosenfeld, K. R. Choudhury, and W. Wu, J. Am. Chem. Soc. **134**, 15644 (2012).
[2]Q. Guo, H. Hillhouse, and R. Agrawal, J. Am. Chem. Soc. **131**, 11672 (2009).
[3]W. Ki and H. W. Hillhouse, Adv. Energy Mater. **1**, 732 (2011).
[4]A. Shavel, D. Cadavid, M. Ibáñez, A. Carrete, and A. Cabot, J. Am. Chem. Soc. **134**, 1438 (2012).
[5]B. Shin, O. Gunawan, Z. Yu, N. A. Bajarzuk, S. J. Chey, and S. Guha, Prog. Photovoltaics: Res. Appl. **21**, 72 (2013).
[6]G. Brammertz, M. Buffière, S. Oueslati, H. ElAnzeery, K. B. Messaoud, S. Sahayaraj, C. Köble, M. Meuris, and J. Poortmans, Appl. Phys. Lett. **103**, 163904 (2013).
[7]W. Shockley and H. J. Queisser, J. Appl. Phys. **32**, 510 (1961).
[8]W. Wang, M. T. Winkler, O. Gunawan, T. Gokmen, T. K. Todorov, Y. Zhu, and D. B. Mitzi, Adv. Energy Mater. **4**, 1301465 (2014).
[9]T. K. Todorov, J. Tang, S. Bag, O. Gunawan, T. Gokmen, Y. Zhu, and D. B. Mitzi, Adv. Energy Mater. **3**, 34 (2013).
[10]S. C. Riha, B. A. Parkinson, and A. L. Prieto, J. Am. Chem. Soc. **133**, 15272 (2011).
[11]A. Singh, S. Singh, S. Levcenko, T. Unold, F. Laffir, and K. M. Ryan, Angew. Chem., Int. Ed. Engl. **52**, 9120 (2013).
[12]K. Yang and M. Ichimura, Int. J. Photoenergy **2012**, 154704 (2012).
[13]T. Washio, T. Shinji, S. Tajima, T. Fukano, T. Motohiro, K. Jimbo, and H. Katagiri, J. Mater. Chem. **22**, 4021 (2012).
[14]C. Tablero, Thin Solid Films **520**, 5011 (2012).
[15]J. Paier, R. Asahi, A. Nagoya, and G. Kresse, Phys. Rev. B **79**, 115126 (2009).
[16]S. Chen, X. G. Gong, A. Walsh, and S.-H. Wei, Appl. Phys. Lett. **94**, 041903 (2009).
[17]S. Chen, A. Walsh, Y. Luo, J.-H. Yang, X. G. Gong, and S.-H. Wei, Phys. Rev. B **82**, 195203 (2010).
[18]S. Chen, J.-H. Yang, X. G. Gong, A. Walsh, and S.-H. Wei, Phys. Rev. B **81**, 245204 (2010).
[19]C. Persson, J. Appl. Phys. **107**, 053710 (2010).
[20]T. Gürel, C. Sevik, and T. Çağın, Phys. Rev. B **84**, 205201 (2011).
[21]T. Maeda, S. Nakamura, and T. Wada, Jpn. J. Appl. Phys. **50**, 04DP07 (2011).
[22]A. Singh, H. Geaney, F. Laffir, and K. M. Ryan, J. Am. Chem. Soc. **134**, 2910 (2012).
[23]H.-R. Liu, S. Chen, Y.-T. Zhai, H. J. Xiang, X. G. Gong, and S.-H. Wei, J. Appl. Phys. **112**, 093717 (2012).
[24]A. Khare, B. Himmetoglu, M. Cococcioni, and E. S. Aydil, J. Appl. Phys. **111**, 123704 (2012).
[25]I. Camps, J. Coutinho, M. Mir, A. F. D. Cunha, M. J. Rayson, and P. R. Briddon, Semicond. Sci. Technol. **27**, 115001 (2012).
[26]A. Walsh, S. Chen, S.-H. Wei, and X.-G. Gong, Adv. Energy Mater. **2**, 400 (2012).
[27]L. Burton and A. Walsh, J. Phys. Chem. C **116**, 24262 (2012).
[28]S. Chen, A. Walsh, X.-G. Gong, and S.-H. Wei, Adv. Mater. **25**, 1522 (2013).
[29]T. Oliveira, J. Coutinho, and V. Torres, Thin Solid Films **535**, 311 (2013).
[30]P. Hohenberg and W. Kohn, Phys. Rev. **136**, B864 (1964).
[31]W. Kohn and L. Sham, Phys. Rev. **140**, A1133 (1965).
[32]J. Perdew and Y. Wang, Phys. Rev. B **45**, 13244 (1992).
[33]P. Blöchl, Phys. Rev. B **50**, 17953 (1994).
[34]P. Giannozzi *et al.*, J. Phys.: Condens. Matter **21**, 395502 (2009).
[35]X. Gonze, B. Amadon, P. M. Anglade, J. M. Beuken, F. Bottin, P. Boulanger, F. Bruneval, D. Caliste, R. Caracas, M. Cote, T. Deutsch, L. Genovese, P. Ghosez, M. Giantomassi, S. Goedecker, D. R. Hamann, P. Hermet, F. Jollet, G. Jomard, S. Leroux, M. Mancini, S. Mazevet, M. J. T. Oliveira, G. Onida, Y. Pouillon, T. Rangel, G. M. Rignanese, D. Sangalli, R. Shaltaf, M. Torrent, M. J. Verstraete, G. Zerah, and J. W. Zwanziger, Comput. Phys. Commun. **180**, 2582 (2009).
[36]N. A. W. Holzwarth, A. R. Tackett, and G. E. Matthews, Comput. Phys. Commun. **135**, 329 (2001).
[37]A. Kokalj, J. Mol. Graphics Modell. **17**, 176 (1999).
[38]K. Momma and F. Izumi, Appl. Crystallogr. **44**, 1272 (2011).
[39]S. Levcenko, V. E. Tezlevan, E. Arushanov, S. Schorr, and T. Unold, Phys. Rev. B **86**, 045206 (2012).
[40]X. Chen, H. Wada, A. Sato, and M. Mieno, J. Solid State Chem. **139**, 144 (1998).
[41]I. Olekseyuk, L. Gulay, I. Dydchak, L. Piskach, O. Parasyuk, and O. Marchuk, J. Alloys Compd. **340**, 141 (2002).
[42]K. Lisunov, M. Guk, A. Nateprov, S. Levcenko, V. Tezlevan, and E. Arushanov, Sol. Energy Mater. Sol. Cells **112**, 127 (2013).

[43]G. Zoppi, I. Forbes, R. Miles, P. Data, J. Scragg, and L. Peter, Prog. Photovoltaics: Res. Appl. **17**, 315 (2009).
[44]S. R. Hall, J. T. Szymanski, and J. M. Stewart, Can. Mineral. **16**, 131 (1978), http://rruff.geo.arizona.edu/AMS/minerals/Stannite.
[45]In *International Tables for Crystallography, Volume A: Space-Group Symmetry*, 5th revised ed., edited by T. Hahn (Kluwer, 2002).
[46]L. Choubrac, M. Paris, A. Lafond, C. Guillot-Deudon, X. Rocquefelte, and S. Jobic, Phys. Chem. Chem. Phys. **15**, 10722 (2013).
[47]A. Redinger, D. M. Berg, P. J. Dale, and S. Siebentritt, J. Am. Chem. Soc. **133**, 3320 (2011).
[48]A. Nagaoka, K. Yoshino, H. Taniguchi, T. Taniyama, and H. Miyake, J. Cryst. Growth **354**, 147 (2012).
[49]E. Engel and S. H. Vosko, Phys. Rev. B **47**, 13164 (1993).
[50]J. P. Perdew, K. Burke, and M. Ernzerhof, Phys. Rev. Lett. **77**, 3865 (1996), Erratum—*ibid.* **78**, 1396 (1997).
[51]J. Heyd, G. E. Scuseria, and M. Ernzerhof, J. Chem. Phys. **118**, 8207 (2003).
[52]S. Botti, D. Kammerlander, and M. A. L. Marques, Appl. Phys. Lett. **98**, 241915 (2011).
[53]In *CRC Handbook of Chemistry and Physics*, 92th ed., edited by W. M. Haynes (CRC Press, Taylor & Francis Group, 2011).
[54]M. W. Chase, Jr., C. A. Davies, J. R. Downey, Jr., D. J. Frurip, R. A. McDonald, and A. N. Syverud, *NIST JANAF Thermochemical Tables 1985* (1986), available online: http://kinetic.nist.gov/janaf.
[55]O. Kubaschewski, C. B. Alcock, and P. J. Spencer, *Materials Thermochemistry*, 6th ed. (Pergamon Press, New York, 1993).
[56]L. Wang, T. Maxisch, and G. Ceder, Phys. Rev. B **73**, 195107 (2006).
[57]N. D. Lepley, N. A. W. Holzwarth, and Y. A. Du, Phys. Rev. B **88**, 104103 (2013).
[58]S. Schorr, Sol. Energy Mater. Sol. Cells **95**, 1482 (2011).
[59]A. Belsky, M. Hellenbrandt, V. L. Karen, and P. Luksch, Acta Crystallogr. B **58**, 364 (2002).
[60]V. Stevanović, S. Lany, X. Zhang, and A. Zunger, Phys. Rev. B **85**, 115104 (2012).
[61]H. Fjellvåg, F. Grønvold, S. Stølen, A. F. Andresen, R. Müller-Käfer, and A. Simon, Z. Kristallogr. **184**, 111–121 (1988).
[62]P. Lukashev, W. Lambrecht, T. Kotani, and M. van Schilfgaarde, Phys. Rev. B **76**, 195202 (2007).
[63]S. Schorr, A. Weber, V. Honkimäki, and H.-W. Schock, Thin Solid Films **517**, 2461 (2009).
[64]H. Yoo and J. Kim, Thin Solid Films **518**, 6567 (2010).
[65]A. Nagoya, R. Asahi, R. Wahl, and G. Kresse, Phys. Rev. B **81**, 113202 (2010).
[66]S. Deka, A. Genovese, Y. Zhang, K. Miszta, G. Bertoni, R. Krahne, C. Giannini, and L. Manna, J. Am. Chem. Soc. **132**, 8912 (2010).
[67]R. Grau-Crespo, S. Hamad, C. R. A. Catlow, and N. H. de Leeuw, J. Phys.: Condens. Matter **19**, 256201 (2007).
[68]J. He, L. Sun, N. Ding, H. Kong, S. Zuo, S. Chen, Y. Chen, P. Yang, and J. Chu, J. Alloys Compd. **529**, 34 (2012).
[69]S. Levcenco, D. Dumcenco, Y. Wang, Y. Huang, C. Ho, E. Arushanov, V. Tezlevan, and K. Tiong, Opt. Mater. **34**, 1362 (2012).
[70]Q. Guo, G. M. Ford, W.-C. Yang, B. C. Walker, E. A. Stach, H. W. Hillhouse, and R. Agrawal, J. Am. Chem. Soc. **132**, 17384 (2010).
[71]R. Schurr, A. Hölzing, S. Jost, R. Hock, T. Voss, J. Schulze, A. Kirbs, A. Ennaoui, M. Lux-Steiner, A. Weber, I. Kötschau, and H.-W. Schock, Thin Solid Films **517**, 2465 (2009).